Journal of Power Sources 197 (2012) 50–56

Contents lists available at SciVerse ScienceDirect

Journal of Power Sources

journal homepage: www.elsevier.com/locate/jpowsour

An experimental study of the liquid water saturation level in the cathode gas diffusion layer of a PEM fuel cell

Xuhai Wang, Trung Van Nguyen*

Department of Chemical and Petroleum Engineering, The University of Kansas, Lawrence, KS 66045, USA

ARTICLE INFO

Article history:
Received 9 July 2011
Received in revised form
13 September 2011
Accepted 15 September 2011
Available online 22 September 2011

Keywords:
PEM fuel cells
Liquid saturation levels
Relative permeability

ABSTRACT

A proton exchange membrane (PEM) fuel cell with a flow field that can be switched between the serpentine and the interdigitated flow modes was used to measure the liquid water saturation level in the gas diffusion layer (GDL) of the cathode and the effect of the liquid water saturation level on the fuel cell performance. Using correlations between the liquid water saturation level and gas relative permeability obtained by neutron imaging, the liquid water saturation level in the GDL under serpentine flow mode was determined by the gas pressure drop across the GDL right after the flow field was switched from the serpentine mode to interdigitated mode. The results showed that the saturation levels in the cathode GDL during the interdigitated mode was much lower than that during the serpentine mode leading to better oxygen gas access to the cathode catalyst layer and consequently better fuel cell performance, especially at high current densities and low oxygen stoichiometric flow rate. In most cases, the fuel cell became unstable when the average liquid water saturation level exceeded 20%.

1. Introduction

Proper water management is crucial to the operations of a proton exchange membrane (PEM) fuel cell. As a part of the membrane electrode assembly (MEA), the gas diffusion layer (GDL) provides transport pathways for electrons, gas, and liquid water from the catalyst layer (CL) to the flow channels and vice versa [1]. Gas diffusion layers that result in low liquid water saturation levels in the GDLs will improve fuel cell performance by allowing faster gas transport to and from the active catalyst sites when the gas transport in the GDL is a dominant factor. Two-phase flow properties such as the capillary pressure and the relative permeability of the porous media greatly affect the liquid water transport rate and the liquid saturation level in the GDL. Modeling results showed that a hydrophobic GDL could contribute to better fuel cell performance by lowering the liquid saturation levels in the GDL [2]. Quantification of the liquid saturation level in the GDL will be useful in validating the predictions of these two-phase flow models and determining the role of liquid water in affecting the fuel cell performance.

Continual efforts have been made to determine the liquid saturation levels in the MEAs of PEM fuel cells. Optical visualization (transparent fuel cell) [3,4], nuclear magnetic resonance (NMR) [5–7], X-ray computed tomography (X-CT) [8,9], and neutron imaging [10–14] were used to determine the liquid water content in PEM fuel cells. Optical visualization requires transparent materials that have different surface wetting and thermal properties with actual materials in a fuel cell and, therefore, has limited applications. The presence of the magnetically inductive carbon powder and fibers in the fuel cell electrodes limits the NMRs application to mainly the membranes of the MEAs. High resolution X-rays are limited by the dimensions of the sample. High resolution neutron imaging is capable of measuring both in-plane and through-plane liquid water distributions in a MEA of a fuel cell. However, limited availability of neutron facility is a major drawback to most users.

He et al. [15] developed a diagnostic tool to study the effect of liquid water saturation level in the GDLs of a PEM fuel cell by taking advantage of the in-plane gas pressure drop in an interdigitated flow mode. The study showed that cathode flooding was the main cause of poor fuel cell performance at high current density. It was also shown that this technique could be used to study the relationship between the liquid water saturation level in the GDL and the rate of gas flowing through the GDL in the in-plane direction as well as the fuel cell operating temperature. However, in the study by He et al., direct quantification of the liquid water content in the GDL was not possible and could only be inferred by the gas phase pressure drop across the GDL. So unless the water content in the GDL was measured directly by some imaging techniques, such as neutron imaging, the alternative way is to have a correlation between the in-plane gas relative permeability and the liquid saturation level in the GDL. That is, if the gas flow rate through a GDL in the in-plane direction and the pressure drop across a GDL in the same direction are known when an interdigitated flow field is used, the gas relative permeability can be calculated. Next, if a correlation of the in-plane gas relative permeability and liquid saturation

* Corresponding author.
E-mail address: cptvn@ku.edu (T.V. Nguyen).

0378-7753/$ – see front matter © 2011 Elsevier B.V. All rights reserved.
doi:10.1016/j.jpowsour.2011.09.036

level is available for this gas diffusion media, the saturation level in the GDL can be determined.

Since experimentally measured relative permeability for both through-plane and in-plane directions and liquid water saturation level correlations are not available, empirical correlations have been used [16–21]. One of these empirical correlations is the 3rd-order power correlation between the liquid saturation level and the relative permeability developed for nonconsolidated and well-sorted sand [22],

$$k_{r,g} = k^0(1-s)^3 \quad (1)$$

where $k_{r,g}$ is the gas relative permeability, k^0 is the absolute permeability, and s is the liquid saturation level in the gas diffusion medium. However, the porous GDLs used in PEM fuel cells are either non-woven papers or woven cloth made of carbon fibers. Furthermore, due to the preferred in-plane orientation of these carbon fibers these carbon-based GDLs often have anisotropic two-phase flow properties. Thus, using the 3rd-order power relative permeability measured for sands often leads to inaccurate predictions of the liquid water saturation level in the GDLs. After the work by He et al. [15], Yamada et al. [23] was the next to apply the approach of using the pressure drop signal across a GDL in the in-plane direction with an interdigitated flow field proposed by Nguyen [24] as a diagnostic tool to study the effect of water flooding in the cathode GDL of a PEM fuel cell.

In recent years, absolute gas permeability of the GDLs used in PEM fuel cells has become available [25–27]. Our group has measured both gas and liquid relative permeability of these carbon-based gas diffusion media by a gravimetric method and an in situ neutron imaging technique [28]. Based on these measurements, correlations between the in-plane relative permeability and the liquid saturation level were developed and recently published in Ref. [28]. In this work, the measured correlations of in-plane relative permeability and liquid water saturation levels in Ref. [28] were applied to a PEM fuel cell with interdigitated flow fields to predict the liquid water saturation levels in the GDLs.

2. Experimental

Fig. 1 shows the PEM fuel cell setup used in this experiment. The main feature is a cathode flow field that could be switched between the serpentine flow mode and interdigitated flow mode. The top and cross-sectional views in Fig. 1a and c show that the gas flow direction in the serpentine mode is mainly along the flow channels. Similar views in Fig. 1b and d show that gas flow in the interdigitated mode, when valve V1 is closed, is mainly through the GDL.

The experimental procedure and details are as follows:

(1) Contrary to the approach used by He et al. [15] the fuel cell in this study was operated in galvanostatic (constant-current) mode to control the consumption and generation rates of reactants and products (i.e., water in the cathode). The rates of gas feed were based on fixed stoichiometric ratios of the total applied electric current. A new MEA was activated by scanning the full polarization curve twice and staying at low voltage 0.4 V for several hours to fully hydrate the membrane. The test began after the MEA was fully activated.

(2) At each current density the fuel cell was first operated under serpentine flow mode. This was achieved with valve V1 in Fig. 1 in the open position. Once the fuel cell performance became steady, the fuel cell was switched to interdigitated flow mode, by closing valve V1 in Fig. 1, and maintained in this mode until its performance also became steady. The current density and gas flow rate were kept the same during both flow modes. Even though it was found during this study that steady state performance was achieved in less than 5 min, the fuel cell was operated for 15 min under each mode. The pressure drop across the GDL, fuel cell voltage, cell temperature, and humidifier temperatures were monitored continuously under both serpentine and interdigitated flow modes.

It was in the interdigitated flow mode in which gas was flown through the GDL between the inlet and outlet channels that the gas pressure drop was measured and the liquid water saturation level was determined. Since the serpentine mode was used first and followed by the interdigitated mode at each current density setting, the gas pressure drop at the instant the cathode flow field was switched from serpentine mode to interdigitated mode correlates with the liquid water saturation level in the GDL of the serpentine mode. The gas pressure drop after the fuel cell reached steady state in the interdigitated mode correlates with the steady state liquid water saturation level in the cathode in the interdigitated mode. This approach allows for the determination of liquid saturation levels in the cathode GDL under the serpentine flow mode and the interdigitated flow mode, respectively. While steady state results were obtained in this study, transient saturation levels in the GDL at any moment in the serpentine mode could be obtained by switching to the interdigitated mode and measuring the instant air pressure drop.

(3) Step 2 was repeated at each current density until the fuel cell reached the mass transport limiting region. In the mass transport limiting region, unstable fuel cell voltage was observed, which ultimately led to fuel cell failure as the cell voltage dropped below 0.1 V under the galvanostatic mode. To prevent fuel and oxidant starvation and fuel cell failure, the flow rates of air and hydrogen were adjusted before the current density was changed from a low current density to a higher current density. Similarly, when the current density was changed from a high level to a lower level, the air and hydrogen flow rates were adjusted after the current density was changed.

(4) Using the measurements obtained in steps 2 and 3, the liquid water saturation levels in the cathode were determined as follows. First, based on the air pressure drop (ΔP_g), the gas viscosity (μ), the gas volumetric flow rate (Q), and the dimensions of the flow field and GDL (the width of the rib or shoulder, Δx, and the cross-sectional area of the GDL above the rib, A) the in-plane gas permeability is calculated as shown in Eq. (2).

$$k_{r,g} = -v_g \mu_g \frac{\Delta x}{\Delta P_g} = -\frac{Q}{A}\mu_g \frac{\Delta x}{\Delta P_g} \quad (2)$$

Next, using the correlations of the in-plane gas relative permeability and liquid water saturation level obtained for the GDLs tested here (see Ref. [28]), the liquid saturation level can be determined.

The gas pressure drop across the GDL was measured by an OMEGA PX 139 (Omega Engineering, Inc.) pressure transducer (±35 kPa) and recorded by a data acquisition system (Personal Daq System by Omega Engineering, Inc.). The fuel cell current was controlled and the voltage was monitored by a computer controlled potentiostat/gavalnostat (Arbin System, Inc.). The temperatures of the fuel cell and humidifiers were kept constant at 70 °C, unless otherwise stated. Nafion 112 membrane was used in the MEAs. Carbon supported platinum catalyst with 20 wt% Pt (Tanaka Kikinzoku Kogyo K. K., Japan) was used. The catalyst loading of each electrode was 0.48 mg Pt cm^{-2}. The MEAs had an active area of 2.08 cm × 0.65 cm or about 1.35 cm^2. The same electrode material was used for the cathode and anode. The MEAs were made by hot compressing the electrodes and the Nafion membrane under

Table 1
Fuel cell operation conditions.

Flow stoichiometry (anode/cathode)	2/4
Fuel cell pressure	1 bar
T_{cell}	70 °C
T_{humid} (anode/cathode)	70/70 °C
Flow configuration	Co-flow

T_{cell} is the temperature of the fuel cell.
T_{humid} is the temperature of the humidifier.

Table 2
Properties of gas transport media used in the experiment.

Material type	Base support layer (BSL)	BSL thickness (μm)	BSL porosity	PTFE content in BSL (wt%)
B1	A1 (proprietary GDL)	216	0.81	0
B3	A3 (proprietary GDL)	325	0.85	5

1.47×10^6 Pa at 135 °C for 5 min. The fuel cell was assembled under 3.78×10^6 Pa.

The dimensions of the flow field were as follows. The gas channels were 2 mm wide and deep and 12 mm long, and the ribs were 2 mm wide. In this experiment, unless otherwise stated, the anode and cathode gas flow stoichiometries were kept at 2 and 4, respectively. Gas co-flow configuration for the anode and cathode was used. During the fuel cell test, the anode was kept in the interdigitated flow mode. The fuel cell operation conditions are summarized in Table 1.

The GDLs were compressed when an MEA was assembled into a fuel cell in order to seal the gases and minimize the electrical contact resistance in the cell. However, the gas relative permeability was tested under a lower compressed condition. It is assumed that compression has the same effect on the absolute permeability and relative permeability. Thus, the relative permeability under one compression level can be calibrated to another compression level using the absolute values at these compressed states. This experiment provides a convenient means to evaluate the in situ saturation levels in porous media of a fuel cell. The correlation developed can be used to determine the saturation levels in other fuel cells as long as the specific porous medium is used.

2.1. Materials

Two types of proprietary GDLs, B1 and B3, were used as gas diffusion media in this experiment. The properties of B1 and B3 are listed in Table 2. The catalyst layers were prepared by applying the Pt/C and Nafion ink onto the porous gas diffusion media (B1 and B3). The cathode and anode electrodes were made of the same materials. The electrodes used in this study were provided by TVN Systems.

B1 is a bi-layer porous medium with the base support layer (BSL) of A1 and a micro-porous layer (MPL) pasted on the base support. Similarly, B3 is a bi-layer porous medium with the base support layer of A3 and an MPL pasted on the base support. Thus, the relative permeability correlations of the GDLs (A1 and A3) measured

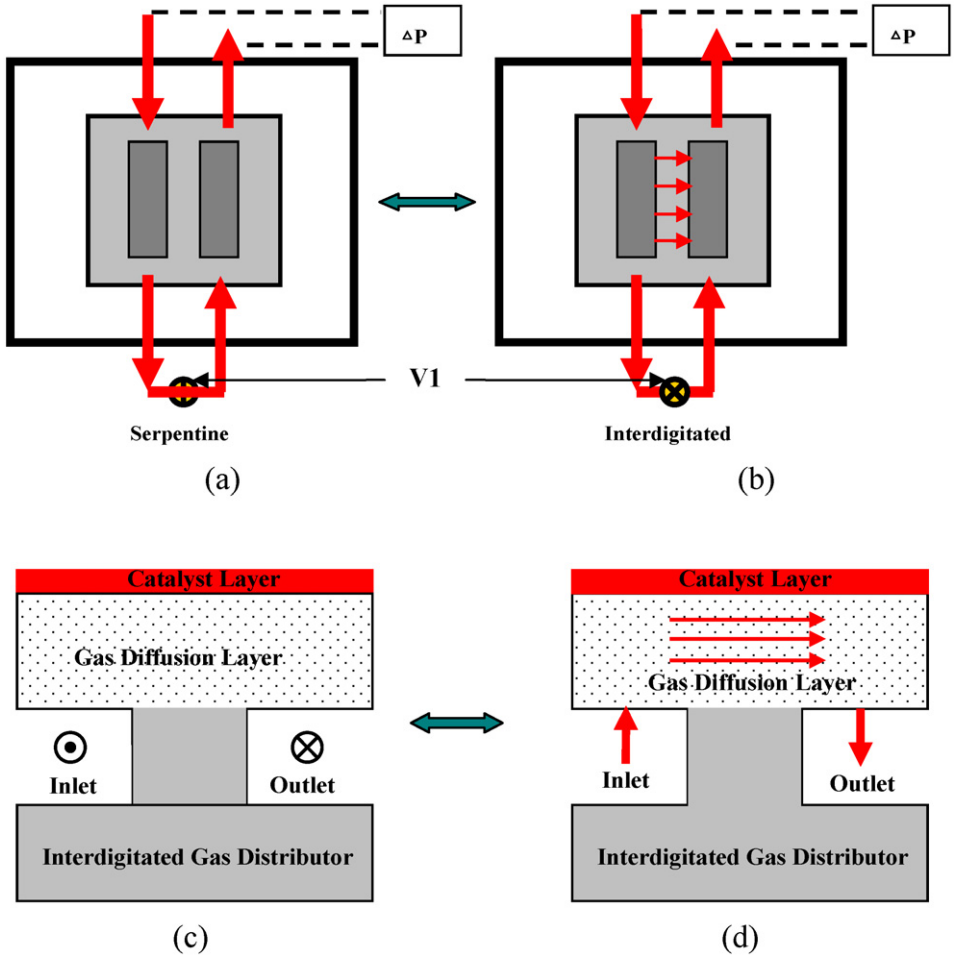

Fig. 1. Schematic of the (a) serpentine and (b) interdigitated flow modes and a cross-sectional view of the (c) serpentine and (d) interdigitated flow fields. (⊙) Gas flowing out of the surface, and (⊗) gas flowing into the surface.

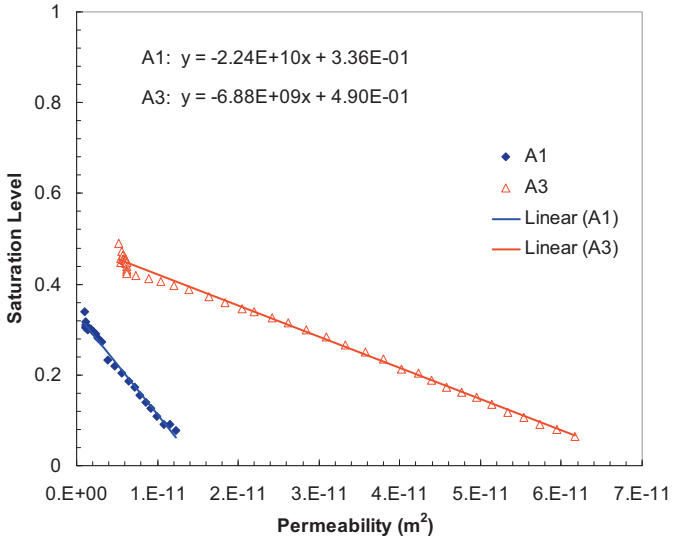

Fig. 2. Correlations between saturation level and permeability of the materials used.

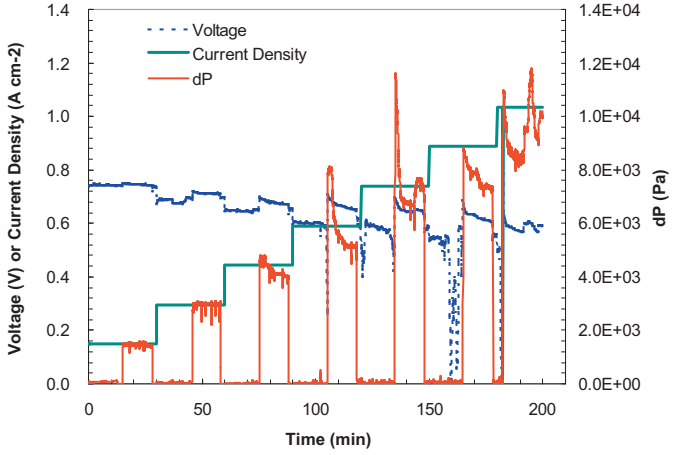

Fig. 3. Voltage, current density, and pressure drop for sample B1. Stoichiometry of A/C = 2/4, temperature of $T_{cell}/T_A/T_C$ = 70/70/70 °C. A and C represent anode and cathode, respectively.

in Ref. [28] can be used in this paper to determine the liquid water saturation levels in the electrode.

2.2. Relative permeability correlations

The correlations between the in-plane gas relative permeability and liquid water saturation level for the two proprietary GDLs used in this study obtained by neutron imaging were given in Ref. [28] as

$$\text{A1}: \quad k_{r,g} = -4.41 \times 10^{-11} s + 1.49 \times 10^{-11} \ \text{m}^2 \tag{3}$$

$$\text{A3}: \quad k_{r,g} = -1.45 \times 10^{-10} s + 7.09 \times 10^{-11} \ \text{m}^2 \tag{4}$$

While correlations by both gravimetric analysis and neutron imaging were obtained, the correlations obtained by neutron imaging were selected because they were considered to be more accurate.

Since Eqs. (3) and (4) are explicit functions of the in-plane gas relative permeability and the liquid water saturation level, in order to determine the liquid saturation level explicitly, as needed in this study, the liquid water saturation levels versus relative permeability data obtained in the study in Ref. [28] were replotted as shown in Fig. 2 and the following correlations of saturation level versus in-plane gas relative permeability were obtained:

$$\text{A1}: \quad s = -2.24 \times 10^{10} k_{r,g} + 0.336 \tag{5}$$

$$\text{A3}: \quad s = -6.88 \times 10^{9} k_{r,g} + 0.490 \tag{6}$$

Note that for the zero wet proof material B1 the gas relative permeability was quite limited once the liquid saturation level exceeded 0.3. For the 5% wet proof material B3 the correlation is linear up to the saturation level of 0.42, beyond which gas relative permeability appeared to change only slightly. Once the in-plane gas relative permeability was obtained from the pressure drop measurement, the saturation level can be calculated using Eqs. (5) and (6). We need to point out here that even though the correlations in Eqs. (5) and (6) were used to calculate the liquid saturation level over the full relative permeability range, the accuracy of the liquid saturation levels beyond the saturation range measured in the neutron imaging study was not certain. Furthermore, the liquid saturation levels calculated in this study should be considered as averaged values of the saturation level distributions within the GDL even though a liquid saturation level gradient is expected to exist along both the through-plane and in-plane directions in the GDL as liquid water is transported out of the catalyst layer to the gas flow channels.

3. Results and discussion

3.1. Base case

The fuel cell voltage, current density and pressure drop versus time for sample B1 for the base case are shown in Fig. 3. First, the pressure drop in the serpentine mode was stable and negligible since the resistance in the flow channel was small due to the short pathway of the channel. Second, two different phenomena were observed in the interdigitated mode: a stable pressure drop at low current density and a decreasing pressure drop at high current density. At low current density, little water accumulated in the porous GDL since the combined water generation rate by the oxygen reduction reaction and electro-osmosis was low. The water saturation levels under serpentine flow and interdigitated flow did not differ much. Thus, the pressure drop under interdigitated flow resulted mainly from gas flow through the dense pore structure of the porous medium. At high current density (>0.5 A cm^{-2}), liquid water accumulated in the porous GDL above the channels and rib during the serpentine flow mode resulting in reduced gas void volume. As the flow mode switched from serpentine to interdigitated, the pressure drop was initially high because of the high liquid water level in the GDL established during the serpentine flow mode. Note that since the gas flow rate is controlled, to maintain this fixed flow rate the pressure has to increase to overcome the higher flow resistance in the GDL created by higher liquid water saturation level. As air flowed through the GDL under the interdigitated mode, the shear force purged part of the liquid water accumulated in the GDL leading to a lower saturation level and lower pressure drop.

Third, the fuel cell voltage under the interdigitated mode was higher than that under the serpentine mode. This higher performance can be attributed to higher reactant pressure or concentration and faster transport of the oxygen reactant to the catalyst layer in the interdigitated flow mode. From previous modeling and imaging studies which showed higher liquid water accumulation above the ribs than above the flow channels when conventional flow fields were used, this increase in performance can be attributed to more area of the catalyst layer above the flow field becoming accessible to oxygen gas and reaction when liquid water in the GDL above the rib region was removed. Finally, the cell voltage under the serpentine mode became unstable at current density 0.9 A cm^{-2} and higher because of excessive

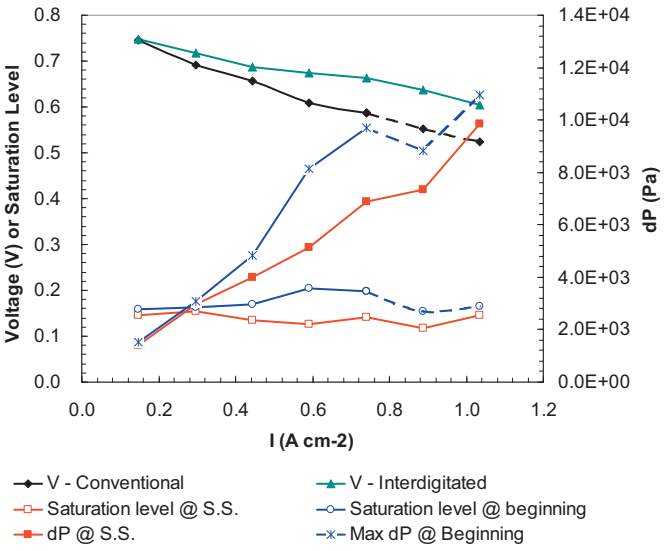

Fig. 4. Fuel cell performance, pressure drop, and saturation level of material B1. Stoichiometry of A/C = 2/4, temperature of $T_{cell}/T_A/T_C$ = 70/70/70 °C.

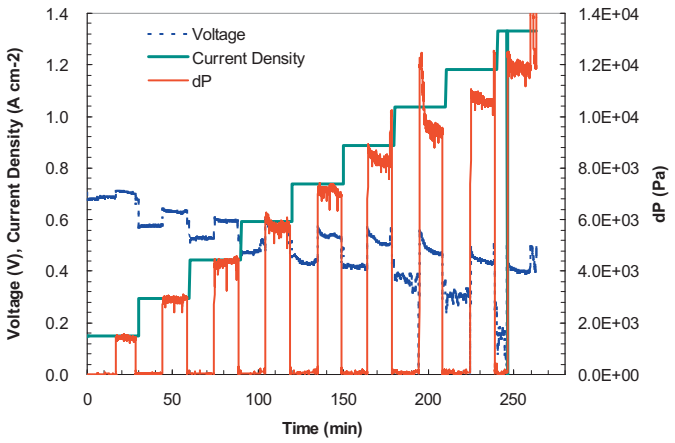

Fig. 5. Voltage, current density, and pressure drop in the test of sample B3. Stoichiometry of A/C = 2/4, temperature of $T_{cell}/T_A/T_C$ = 70/70/70 °C.

accumulated liquid water in the cathode GDL at these current densities. The voltage under the interdigitated flow mode was stable because the shear force from air flow through the GDL effectively reduced the liquid water saturation level in the GDL leading to faster gas transport through the GDL.

The fuel cell performance, gas pressure drop at the beginning and at the steady state of the interdigitated flow mode, and calculated saturation level corresponding to the gas pressure drop across sample B1 are shown in Fig. 4. The gas relative permeability was calculated based on the pressure drop between the air inlet and outlet using Eq. (2), and the saturation level was calculated using Eqs. (5) and (6) after the permeability was calculated.

The interdigitated flow mode showed better fuel cell performance because the GDL under this mode had lower saturation level and higher transport rate of the reactant. The gas pressure drop increased with current density as expected because of higher gas flow rates. Saturation level at the beginning of the interdigitated mode represents the saturation level established under the serpentine flow mode. The difference in the gas pressure drop between the beginning and the steady state of the interdigitated mode is attributed to the liquid water saturation level displaced by the air flow under the interdigitated mode. Under the serpentine flow mode, the highest saturation level was reached in the current density range of 0.6–0.8 A cm^{-2}. Beyond 0.8 A cm^{-2}, the fuel cell became unstable, which resulted in the cell voltage dropping to 0.1 V triggering the setup, for safety and to protect the fuel cell, to immediately switch to the interdigitated flow. When the cell voltage dropped too fast the cell would be momentarily switched to open circuit before the load was reengaged as shown in some of the later case studies. In the instances when the cell was switched prematurely out of the serpentine flow mode because of poor performance the liquid water saturation level in the GDL was lower because the operation time under serpentine flow mode was much shorter. The points connected by the dashed lines in Fig. 4 represent the fuel cell voltage, saturation levels and gas pressure drops obtained under unstable operation of the fuel cell. The critical saturation level at which the fuel cell began to fail under serpentine flow mode appears to be around 0.2. Note that the saturation level obtained in this arrangement represents the average liquid water level over the whole thickness of the GDL. The actual liquid saturation level near the micro-porous layer (MPL) or catalyst layer could have been much higher. Note also that this technique cannot determine the liquid saturation levels in the MPL and the CL in the current configuration.

The liquid saturation levels in the GDL under the interdigitated flow mode remained about the same at these current densities showing that the interdigitated flow was very effective in removing liquid water from the GDL. At high current densities, the saturation levels were even slightly lower than those at low current densities. This was caused by the higher air flow rate under stoichiometric flow control, which brought greater shear force to displace liquid water in the cathode GDL.

The voltage, current density, and pressure drop of sample B3 are presented in Fig. 5. Similar phenomena as those in the measurement of sample B1 were observed here. First, the gas pressure drop under the serpentine flow mode was stable and negligible. Under the interdigitated flow mode, at low current density the pressure drop was stable because little liquid water accumulated in the GDL. The difference in the pressure drop between the beginning value and steady state value under the interdigitated flow mode increased when the current density reached 0.60 A cm^{-2} and higher showing that more liquid water started to accumulate in the GDL under the serpentine flow mode at these current densities. Second, the fuel cell voltage under the serpentine flow mode began to fluctuate at the current density of 1.04 A cm^{-2} for this GDL. At the current density of 1.18 A cm^{-2} and higher, the fuel cell under serpentine flow mode failed because the high liquid water saturation level inside the GDL prevented the oxygen gas from reaching the CL to support the electrochemical reaction.

Fig. 6 shows that better fuel cell performance was obtained with the interdigitated flow mode. As discussed earlier in this paper, the less flooded cathode under interdigitated flow mode led to better fuel cell performance. The saturation level under serpentine flow mode was highest at the current density of 1.04 A cm^{-2}. When the current density was 1.18 A cm^{-2} and higher the fuel cell became unstable. As before, the calculated liquid saturation levels at higher current density were lower because the fuel cell failed before it reached steady state, which resulted in less liquid water accumulated inside the GDL. Under the interdigitated flow mode, the calculated liquid saturation levels decreased slightly with the increase of the current density. This was caused by the increased air flow rate at higher current density since the fuel cell was operated in galvanostatic and constant stoichiometric flow rate mode. The increased air flow rate removed more liquid water from the porous GDL. The difference in the gas pressure drop between the serpentine flow mode and the interdigitated flow mode was very small at low current densities since little liquid water existed inside the GDL. This difference

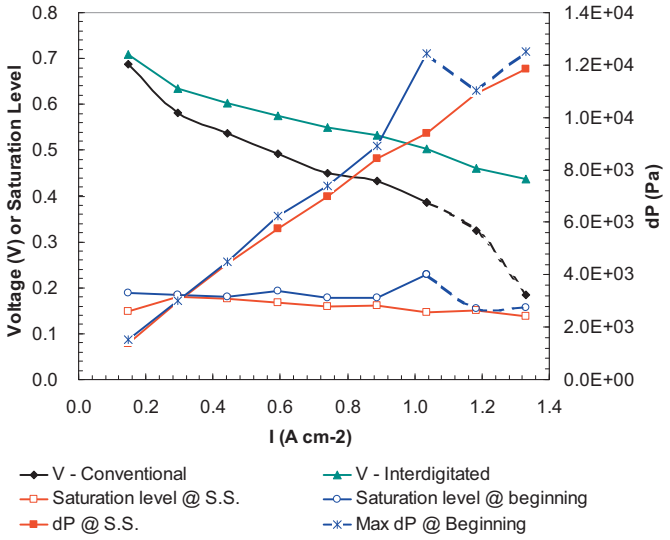

Fig. 6. Fuel cell performance, pressure drop, and saturation level of material B3. Stoichiometry of A/C = 2/4, temperature of $T_{cell}/T_A/T_C$ = 70/70/70 °C.

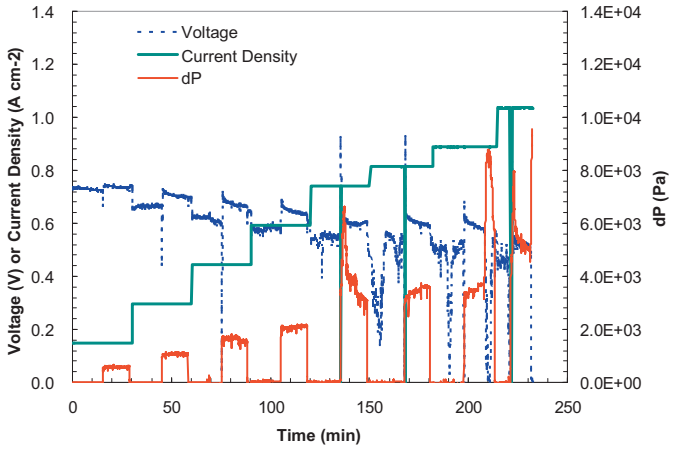

Fig. 7. Voltage, current density, and pressure drop in the test of sample B1. Stoichiometry of A/C = 2/1.5, temperature of $T_{cell}/T_A/T_C$ = 70/70/70 °C.

became more apparent at higher current densities due to higher levels of accumulated water in the cathode GDL. Note also that the liquid water saturation levels were lower and the fuel cell performance was much higher with this GDL (B3) which has a wet-proof gas diffusion substrate (A3). Current densities up to 1.0 A cm^{-2} could be achieved with ambient pressure operation as compared to current densities below 0.8 A cm^{-2} obtained with the GDL (B1) with a non wet-proof gas diffusion substrate (A1). The critical saturation level (s = 0.23) was not reached until the current density exceeded 1.0 A cm^{-2}.

The main uncertainties of this technique come from the dimension changes of the gas diffusion media under compression and the non-uniform distribution of the liquid water saturation level in the gas diffusion media. In a fuel cell, the GDLs are compressed leading to reduced porosity and permeability. If the correlation between the permeability and saturation level was obtained under a different compression level, this effect would need to be accounted for. In our experiment, this uncertainty was minimized by including the compression effect on the absolute permeability. We attributed most of the uncertainty in our study to the non-uniform distribution of liquid water in the GDL. We cannot specify the level of uncertainty from the effect of non-uniform distribution of liquid water because the distribution of liquid water in the GDL is not known using this technique. This could only be obtained by running the same experiment with in situ neutron imaging, something that we will consider in our future study.

3.2. Gas flow stoichiometric effect

The effect of the gas flow stoichiometry was investigated with a lower cathode flow rate while the other operating conditions were kept the same. The purpose was to see how these GDLs performed and what liquid water saturation level existed in these GDLs at low air stoichiometric flow rates. Instead of an air flow stoichiometry of 4 in the cathode side, a lower stoichiometric flow rate of 1.5 was used. Both MEAs consisted of B1 and B3 materials were tested under lower cathode air stoichiometry. However, only the results of the B1 material were presented in this paper for the purpose of brevity. The results of the material B3, although not shown here, showed similar characteristics to those of B1.

Fig. 7 shows that the cathode gas pressure drop under interdigitated flow decreased greatly when the cathode gas flow stoichiometry decreased from 4 to 1.5 (refer to Fig. 3). Compared to the base case, the liquid saturation level was higher in the GDL when the cathode stoichiometry was lower. Voltage oscillation was observed when the current density was about 0.74 A cm^{-2} because of excessive accumulated liquid water in the GDL. A large pressure drop was observed when the fuel cell switched from serpentine flow to interdigitated flow at 0.74 A cm^{-2}. As the liquid water was removed by the shear force of the gas flow, the gas pressure drop decreased gradually. More frequent oscillations were observed and the fuel cell became highly unstable when the current density was increased to the next level. This showed that a higher cathode gas flow stoichiometry was needed to achieve a stable fuel cell performance at current densities beyond 0.74 A cm^{-2} for this GDL at these operating conditions. However, since higher cathode gas flow stoichiometry may result in higher parasitic energy loss, in practice, an optimal gas flow stoichiometry needs to be found.

The fuel cell performances and pressure drops under conventional and interdigitated flow at low air flow stoichiometry are summarized in Fig. 8. Under serpentine flow, the fuel cell performance became unstable at the current densities of 0.74 A cm^{-2} and higher. This unstable point came earlier than when the fuel cell was operated with cathode air flow stoichiometry of 4 (refer to Fig. 4).

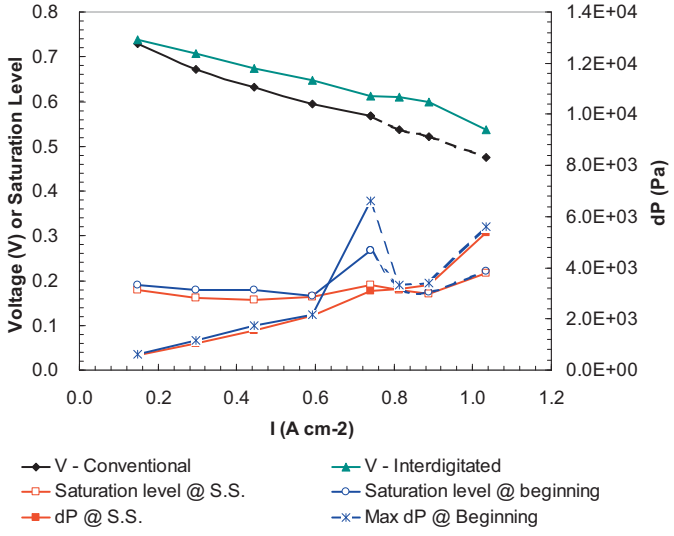

Fig. 8. Fuel cell performance, pressure drop, and saturation level of material B1. Stoichiometry of A/C = 2/1.5, temperature of $T_{cell}/T_A/T_C$ = 70/70/70 °C.

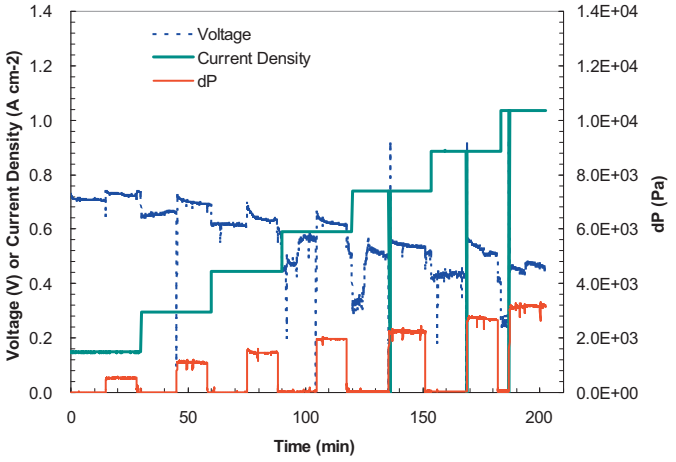

Fig. 9. Voltage, current density, and pressure drop in the test of sample B1. Stoichiometry of A/C = 2/1.5, temperature of $T_{cell}/T_A/T_C$ = 70/50/50 °C.

3.3. *Effects of feed gas temperature and relative humidity*

The effects of feed gas temperature and relative humidification on the fuel cell performance and the cathode pressure drop are shown in Figs. 9 and 10. Note that these effects were investigated at a lower cathode air stoichiometric flow rate of 1.5. The temperature configuration was held at $T_{cell}/T_A/T_C$ = 70/50/50 °C. Since the cathode and anode humidifier temperatures (T_A/T_C = 50/50 °C) were lower than that of the fuel cell (T_{cell} = 70 °C), evaporation in the cathode was expected, which alleviated the flooding effect in the cathode. The calculated liquid water saturation levels in Fig. 10 showed that lower saturation levels existed in the GDL when the cathode was supplied with unsaturated gas. The difference in the beginning and steady state pressure drop under interdigitated flow in this case was relatively small all the way up to the current density of 0.88 A cm^{-2}. This shows that the liquid saturation level in the cathode GDL was quite small and probably not the cause for fuel cell failure at the next higher current density. Instead, anode and membrane dehydration was suspected to be the cause of the fuel cell failure at the current density of 1.04 A cm^{-2}.

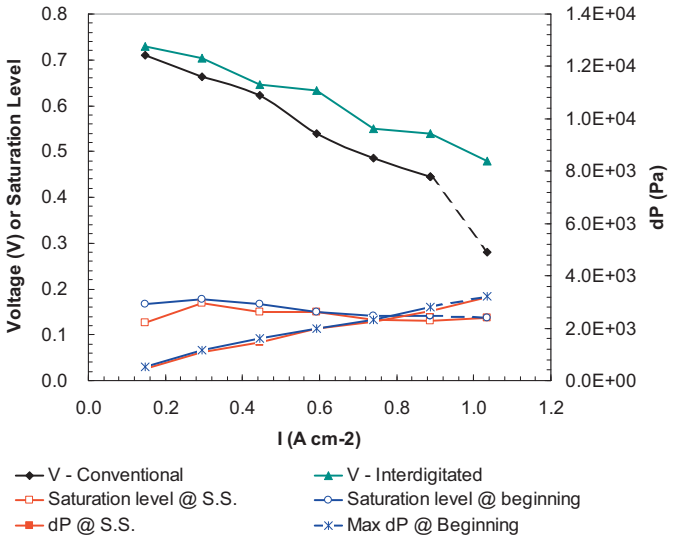

Fig. 10. Fuel cell performance, pressure drop, and saturation level of material B1. Stoichiometry of A/C = 2/1.5, temperature of $T_{cell}/T_A/T_C$ = 70/50/50 °C.

4. Conclusions

Liquid water saturation levels in the cathode GDL of a PEM fuel cell were quantitatively determined using the experimentally measured correlations of the in-plane relative permeability and saturation levels by neutron imaging. By using a fuel cell with a cathode flow field that can be switched from the conventional serpentine flow to interdigitated flow, the liquid saturation levels in the cathode GDL under the serpentine flow mode and interdigitated flow mode can be determined from the gas pressure-drop-across-the-GDL signals. The interdigitated flow led to better fuel cell performance than the conventional serpentine flow because it was more effective in removing liquid water in the gas diffusion layer. The critical average saturation level that led to unstable fuel cell performance under serpentine flow mode appeared to be around 0.2. Lower cathode gas flow stoichiometry led to unstable fuel cell performance at an earlier stage (lower current densities) because the gas phase was less capable of removing liquid water at lower gas flow rate. When the fuel cell was supplied with unsaturated gases, better fuel cell performance benefited from water removal by evaporation in the cathode side. However, when the anode side was less saturated with water vapor, membrane dehydration might limit the fuel cell performance. Finally, this approach can serve as a very useful diagnostic tool to determine the effect of liquid water saturation level in the cathode on the performance of a PEM fuel cell and liquid water saturation levels in the GDLs when the relationship between the in-plane gas relative permeability and liquid saturation level of the GDLs is known.

Acknowledgement

The authors wish to gratefully acknowledge the financial support of this work by Toyota Motor Corporation.

References

[1] M.F. Mathias, J. Roth, J. Fleming, W. Lehnert, in: W. Vielstich, H.A. Gasteiger, A. Lamm (Eds.), Handbook of Fuel Cells – Fundamentals, Technology and Applications, John Wiley & Sons, Ltd., 2003, p. 517.
[2] X. Wang, T.V. Nguyen, J. Electrochem. Soc. 157 (2010) B496.
[3] K. Tuber, D. Pocza, C. Hebling, J. Power Sources 124 (2003) 403.
[4] F.Y. Zhang, X.G. Yang, C.Y. Wang, J. Electrochem. Soc. 153 (2006) A225.
[5] K.W. Feindel, S.H. Bergens, R.E. Wasylishen, ChemPhysChem 7 (2006) 67.
[6] K. Teranishi, S. Tsushima, S. Hirai, J. Electrochem. Soc. 153 (2006) A664.
[7] S. Tsushima, K. Teranishi, S. Hirai, Electrochem. Solid-State Lett. 7 (2004) A269.
[8] P.K. Sinha, P. Halleck, C.-Y. Wang, Electrochem. Solid-State Lett. 9 (2006) A344.
[9] W. Zhu, Z.W. Dunbar, R.I. Masel, ECS Trans. 16 (2008) 995.
[10] A.B. Geiger, A. Tsukada, E. Lehmann, P. Vontobel, A. Wokaun, G.G. Scherer, Fuel Cells 2 (2002) 92.
[11] D.S. Hussey, D.L. Jacobson, M. Arif, J.P. Owejan, J.J. Gagliardo, T.A. Trabold, J. Power Sources 172 (2007) 225.
[12] T. Kim, J. Kim, C. Sim, S. Lee, M. Kaviany, S. Son, M. Kim, Nucl. Instrum. Meth. A 600 (2009) 325.
[13] T. Kim, J. Kim, C. Sim, S. Lee, Y. Son, M. Kim, Nucl. Eng. Technol. 41 (2009) 135.
[14] R. Satija, D.L. Jacobson, M. Arif, S.A. Werner, J. Power Sources 129 (2004) 238.
[15] W. He, G. Lin, T.V. Nguyen, AIChE J. 49 (2003) 3221.
[16] W. He, J.S. Yi, T.V. Nguyen, AIChE J. 46 (2000) 2053.
[17] G. Lin, W. He, T.V. Nguyen, J. Electrochem. Soc. 151 (2004) A1999.
[18] D. Natarajan, T.V. Nguyen, J. Electrochem. Soc. 148 (2001) A1324.
[19] U. Pasaogullari, C.-Y. Wang, K.S. Chen, J. Electrochem. Soc. 152 (2005) A1574.
[20] A.Z. Weber, R.M. Darling, J. Newman, J. Electrochem. Soc. 151 (2004) A1715.
[21] Q. Ye, T.V. Nguyen, J. Electrochem. Soc. 154 (2007) B1242.
[22] M. Kaviany, Principles of Heat Transfer in Porous Media, Springer-Verlag, New York, 1995, p. 708.
[23] H. Yamada, T. Hatanaka, H. Murata, Y. Morimoto, J. Electrochem. Soc. 153 (2006) A1748.
[24] T.V. Nguyen, J. Electrochem. Soc. 143 (1996) L103.
[25] V. Gurau, M.J. Bluemle, E.S. De Castro, Y.-M. Tsou, T.A. Zawodzinski Jr., J.A. Mann Jr., J. Power Sources 165 (2007) 793.
[26] J. Ihonen, M. Mikkola, G. Lindbergh, J. Electrochem. Soc. 151 (2004) A1152.
[27] M.V. Williams, E. Begg, L. Bonville, H.R. Kunz, J.M. Fenton, J. Electrochem. Soc. 151 (2004) A1173.
[28] X. Wang, T.V. Nguyen, D. Hussey, D. Jacobson, M. Arif, J. Electrochem. Soc. 157 (2010) B1777.